

# Electron density studies of porphyrins and phthalocyanines. IV. Electron density distribution in crystals of (meso-tetraphenylporphinato) iron(II)

K. Tanaka,<sup>a)</sup> E. Elkaim, Liang Li,<sup>b)</sup> Zhu Nai Jue,<sup>c)</sup> and P. Coppens<sup>d)</sup>  
*Department of Chemistry, State University of New York at Buffalo, Buffalo, New York 14214*

J. Landrum  
*Department of Chemistry, Florida International University, Miami, Florida 33199*

(Received 2 December 1985; accepted 7 March 1986)

The electron density distribution in crystals of (meso-tetraphenylporphinato)iron(II) has been analyzed using accurate x-ray diffraction data collected at 120 K. The structural results are in agreement with those of the room temperature study. Theoretical calculations predict several different ground states for the complex and in particular support the  ${}^3A_{2g}$  and the  ${}^3E_gA$  states. The experimental electron density distribution shows large peaks above and below the iron atom which would not be present for a  ${}^3E_gA$  ground state. Comparison with Mössbauer quadrupole splittings and the result of the aspherical atom refinement indicate that the axial peaks may be systematically too high in this acentric crystal structure. Nevertheless, it is concluded that their presence indicates a relatively small contribution of the  ${}^3E_gA$  state to the ground state of the complex. This implies that the ground state of FeTPP is different from that of iron(II)phthalocyanine in the crystal. A significant population of electrons is found in the  $d_{x^2-y^2}$  orbital which is mainly attributed to  $\sigma$  donation of electrons from the porphyrin ligand.

## INTRODUCTION

Notwithstanding a large number of studies, the nature of the ground state of the intermediate spin state four-coordinate iron(II) porphyrins and phthalocyanines remains controversial. Experimental techniques which have been used to elucidate the electronic state of these complexes include magnetic susceptibility measurements,<sup>1-3</sup> Mössbauer,<sup>4,5</sup> proton-NMR,<sup>6,7</sup> resonance Raman spectroscopy,<sup>8</sup> and magnetic circular dichroism.<sup>9</sup> Theoretical treatments include an early extended Hückel calculation,<sup>10,11</sup> and more recently SCF-HF,<sup>12,13</sup> SCF with Slater exchange,<sup>14</sup> scattered wave  $X\alpha$ ,<sup>15</sup> and SCF-HF with configuration interaction calculations.<sup>16</sup>

Most recent studies agree that both the  ${}^3A_{2g} [(d_{xy})^2 (d_{xz,yz})^2 (d_z)^2]$  [see also Table VIII(B)] and the  ${}^3E_gA [(d_{xy})^2 (d_{xz,yz})^3 (d_z)^2]$  states are low lying and separated by an energy which is typically estimated to be 600–800  $\text{cm}^{-1}$ . While most studies conclude the  ${}^3A_{2g}$  state to be the lowest in energy, the  ${}^3E_gA$  state is supported by the early extended Hückel calculation,<sup>10,11</sup> the resonance Raman study,<sup>8</sup> and the theoretical treatment by Obara and Kashiwagi.<sup>12</sup> The latter calculation indicates the potential importance of a contribution from a second  ${}^3E_g$  state, labeled  ${}^3E_gB [(d_{xy})^1 (d_{xz,yz})^3 (d_z)^2]$ . Since the measured magnetic moments of 4.2,<sup>17</sup> 4.4,<sup>3</sup> and 4.75  $\mu\text{B}$ <sup>1</sup> are far from the spin only value for a  $S = 1$  state (2.8  $\mu\text{B}$ ), there is a sig-

nificant orbital contribution, and the various electronic configurations are expected to mix through spin-orbit coupling such that the true ground state will be a mixture of several SCF configurations. Calculations by Mispelter, Momen-teau, and Lhoste<sup>7</sup> have further shown that a small axial perturbation can induce a reversal of the ground state, with the  ${}^3A_{2g}$  state increasing in energy relative to the  ${}^3E_gA$  state. For example, the presence of two benzene rings at 3 Å above the iron atom in some so-called "basket-handle" porphyrins causes a change of 650  $\text{cm}^{-1}$  in the relative energies of the two leading contenders for the ground state configuration. The small energy difference and the sensitivity to the environment imply that ground states may differ significantly between solid state and solution, or indeed between solutions in different solvents.

Our analysis of the experimental charge distribution of iron(II) phthalocyanine<sup>18</sup> gave support to a ground state configuration with a major contribution from the  ${}^3E_gA$  state. However, the crystal packing forces in FePc and FeTPP differ significantly, in particular with respect to the axial direction. In FePc a nitrogen atom of an adjacent molecule is located at 3.42 Å from the Fe atom in this direction, whereas no such pseudocoordination occurs in FeTPP. It is therefore entirely possible that the ground states of the two complexes in the solid differ from each other.

To obtain further insight in the ground state properties of the four-coordinate intermediate spin iron complexes we have undertaken a charge density study of FeTPP, which is reported here.

This work is part of a series of electron density studies on metal porphyrins which aim at establishing the nature of the electronic ground state as a function of spin state, coordination number, and valency, which is relevant to the biological action of heme proteins. Previous studies have included CoTPP,<sup>19</sup> Fe(III)OMeTPP<sup>20</sup>, and Fe(II)(THF)<sub>2</sub>TPP.<sup>21</sup>

<sup>a)</sup> Permanent address: Research Laboratory of Engineering Materials, Tokyo Institute of Technology, Nagatsuta 4259, Midori-ku, Yokohama 227, Japan.

<sup>b)</sup> Permanent address: Institute of Biophysics Academia Sinica, Beijing, People's Republic of China.

<sup>c)</sup> Permanent address: Institute of Chemistry, Academia Sinica, Beijing, People's Republic of China.

<sup>d)</sup> Author to whom correspondence should be addressed.

## EXPERIMENTAL

### Data collection

A truncated tetragonal–bipyramidal crystal with a basal edge of 0.48 mm and a height of 0.29 mm was used for the low order ( $\sin \theta / \lambda < 0.70 \text{ \AA}^{-1}$ ) intensity measurements. It was sealed in a Pyrex capillary with wall thickness of 0.1 mm and inner diameter of 0.5 mm to prevent oxidation during the three month measurement period. Unit cell dimensions were obtained by least-squares refinement using the  $\theta$  angles of 25 reflections with  $2\theta < 45^\circ$  (MoK $\alpha$  radiation). X-ray intensity data were collected with  $\theta$ – $2\theta$  scan on a CAD4 four-circle diffractometer at a temperature of  $120 \pm 5 \text{ K}$ . A stream of cold nitrogen gas was used for cooling. The intensity collection was done in two stages. First an octant of reciprocal space with  $\sin \theta / \lambda < 0.702 \text{ \AA}^{-1}$  was collected. After completion of the least-squares refinement of these low order data, an octant was measured in the range of  $0.702 < \sin \theta / \lambda < 0.914 \text{ \AA}^{-1}$ . As the first crystal had deteriorated, a second crystal of approximate dimensions  $0.55 \times 0.41 \times 0.39 \text{ mm}$  along  $a$ ,  $b$ , and  $c$ , respectively, was used for this part of the data collection. The slightly larger size of this second specimen crystal allowed collection of weak high order reflections for which extinction is negligible. Since the linear absorption coefficient is small,  $\mu r$  is less than 0.15, so absorption corrections are not excessive. Additional reflections with calculated intensity larger than  $5\sigma I$  were measured in the range of  $0.914 < \sin \theta / \lambda < 1.22 \text{ \AA}^{-1}$ . The total number of observed reflections was 13 161. Crystal data and experimental conditions are summarized in Table I.

### Data reduction

The step-scan profile of each reflection was integrated to give the intensity as described elsewhere.<sup>22</sup> Standard reflections were measured at regular intervals to correct for intensity fluctuation during the period of measurement. Standard deviations were obtained from the fluctuation of the standard reflections combined with the effect of counting statistics.<sup>23</sup> Corrections for absorption and inhomogeneous beam

profile were made using the Gaussian integration method.<sup>24</sup> Absorption in the capillary was corrected with a modification of our absorption program written by Hansen.<sup>25</sup> Symmetry equivalents were averaged to give 2473 reflections with  $I_{\text{obs}} > 3\sigma I_{\text{obs}}$  which were used in the least-squares refinements.

### Least-squares refinements

Room temperature atomic parameters<sup>3</sup> were used as a starting set in the least-squares refinement with low order data. All the hydrogen atoms were refined with isotropic temperature parameters. Since the low and high order data were not collected on the same crystal and the x-ray tube was changed during the interruption, two scale factors were refined, which differ by only 1% in the final refinement.

The data were first refined with the spherical atom formalism. The free atom scattering factors of Fe, C, N were taken from *International Tables for X-ray Crystallography*,<sup>26</sup> and those of the H atoms were as given by Stewart, Davidson, and Simpson.<sup>27</sup> As extinction was small it was treated isotropically. This refinement (I) led to  $R$  factors  $R = \sum |F_0| - |F_c| / \sum |F_0|$  and  $R_w = \sum w |F_0| - |F_c| / \sum w |F_0|$  of 0.044 and 0.038, respectively. A stereoview of the molecule given in Fig. 1 clearly shows the nonplanarity of the porphyrin ligand, which is ruffled with considerable deviations from the best molecular plane.

The aspherical atom multipole refinement (II) was applied as described by Hansen and Coppens.<sup>28</sup> The atomic density is expressed in terms of an expansion of atom-centered spherical harmonics, the radial part of which contains an expansion–contraction parameter, which is varied in the least-squares treatment together with the populations of the multipole functions. Scattering factors for core electrons and the spherical valence electron function were taken from Ref. 26. Slater-type functions with variable exponent are used for the higher order multipoles, except for the iron atom for which isolated atom Hartree–Fock radial functions, modified by a  $\kappa$  parameter, were used. In this respect the refinement differs from the earlier analysis of FePc. We believe that the consistent use of isolated atom HF radial functions for both the spherical and the deformation terms of the  $d$ -orbital density, proposed by Hansen,<sup>25</sup> is an improvement over the earlier treatment.

Starting values of  $\zeta$ , the orbital exponent of the C and N Slater functions, were taken from the table by Clementi and Raimondi.<sup>29</sup> The  $x$  and  $z$  axes of the local Fe coordinate system were taken along the Fe–N bond and along the direction perpendicular to the porphyrin plane. The coordinate systems for the other atoms except C<sub>7</sub> to C<sub>11</sub> are depicted in Fig. 2 together with the numbering of atoms in the molecule. The  $z$  axes for C<sub>7</sub> to C<sub>11</sub> were taken perpendicular to the phenyl plane, while the  $x$  axes of these atoms were along the direction from each atom to C<sub>6</sub>, C<sub>7</sub>, C<sub>8</sub>, C<sub>11</sub>, and C<sub>6</sub>, respectively. The number of parameters was reduced further by the use of molecular symmetry. Mirror planes were assumed perpendicular to the porphyrin plane through the Fe–N bonds, through the porphyrin plane and through the phenyl ring. The resulting symmetry of the Fe, N, and all C atoms is  $D_{4h} - 4/mmm$ , C<sub>2v</sub>– $mm2$ , and C<sub>s</sub>– $m$ , respectively. Allowed  $d$ -orbi-

TABLE I. Experimental data (tetraphenylporphyrin) iron(II) (FeTPP).

FeTPP	C <sub>44</sub> H <sub>28</sub> N <sub>4</sub> Fe
Space group	$I\bar{4}2d$
Temp, K	120(5)
Cell dimensions	
$a$ , Å	14.996(3)
$c$ , Å	13.777(5)
$V$ , Å <sup>3</sup>	3098(2)
$Z$	4
X-ray wavelength, MoK $\alpha$ , Å	0.710 69
$d$ (calc), g/cm <sup>3</sup>	1.391
Abs. coeff., cm <sup>−1</sup>	5.24
Scan mode	$\theta$ – $2\theta$ step scan
Scan width, deg	$1.5 + 0.525 \tan \theta$
Detector aperture, mm	$9 \times 9$
First crystal size, mm (pyramidal)	$0.49 \times 0.49 \times 0.29(h)$
Second crystal size, mm	$0.55 \times 0.41 \times 0.34(h)$
( $\sin \theta / \lambda$ ) max, Å <sup>−1</sup>	1.22
Number of observed reflections	13 161
Number of reflections with $I > 3\sigma(I)$	2473

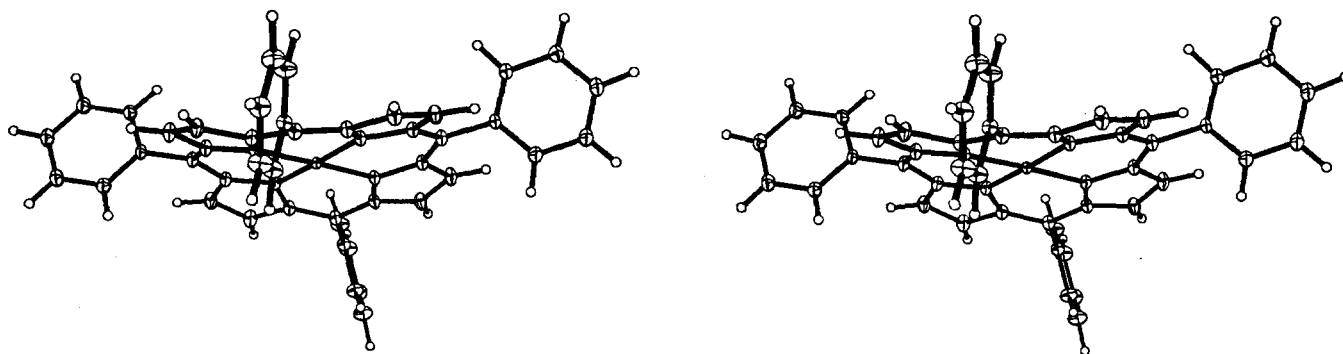


FIG. 1. Stereoview of the molecule showing the deviations from planarity of the porphyrin skeleton.

tal multipole parameters for each symmetry are as summarized by Holladay, Leung, and Coppens.<sup>30</sup> Identical multipole parameters were assigned to all the carbon atoms in the benzene ring except C<sub>6</sub>, the atom adjacent to the meso carbon atom, and to all H atoms. The final agreement factors  $R$ ,  $R_w$ , and goodness of fit  $G$  are 0.036, 0.027, and 1.13, respectively. Tables of observed and calculated structure factors have been deposited in PAPS.<sup>39</sup>

## RESULTS AND DISCUSSION

### Crystal structure

Coordinates and temperature parameters obtained after the final aspherical atom refinement are summarized in Tables II and III. Bond lengths and angles, listed in Tables IV and V, are not significantly different from room temperature values.<sup>3</sup> The Fe–N bond distance is in the range of those in low and intermediate spin iron porphyrins.<sup>31</sup> The distance of atoms from the average molecular plane through the Fe atom, hereafter abbreviated as the porphyrin plane, and planes of pyrrole and phenyl rings are listed in Table VI. FeTPP has a ruffled structure as shown in Fig. 1. The dihedral angles between the porphyrin and the pyrrole planes, and between the porphyrin and the benzene planes are 11.0°

and 77.2°, respectively. The shortest intermolecular distances to the Fe atom are with the benzene ring atoms C<sub>10</sub>, C<sub>11</sub>, and the corresponding hydrogen atoms in a molecule related by the symmetry operation  $-x, y - 1/2, 1/4 - z$ . They are 3.986(2), 3.323(21), 3.931(2), and 3.231(22) Å for C<sub>10</sub>, H<sub>10</sub>, C<sub>11</sub>, and H<sub>11</sub>, respectively. Since the Fe atom is located on a fourfold inversion axis each of the distances is repeated four times. The vector from C<sub>10</sub>, H<sub>10</sub>, C<sub>11</sub>, and H<sub>11</sub> to the Fe atom have angles with the porphyrin plane, 64.2°, 58.7°, 55.7°, and 45.3°, respectively. Since none of the distances is unusually short no axial coordination to the tetra-coordinate Fe atom is considered in the present study. This contrast with FePc in which nitrogen atoms are located at 3.42 Å above and below the Fe atom.

### Electron density maps

The deformation density is defined as

$$\Delta\rho(r) = \frac{1}{V} \sum_{-H}^{+H} \{ |F_{\text{obs}}| \exp(i\phi) - |F_{\text{calc,sph}}| \exp(i\phi_{\text{calc,sph}}) \} \exp(-2\pi i \mathbf{H} \cdot \mathbf{r}),$$

where  $|F_{\text{obs}}|$  and  $|F_{\text{calc,sph}}|$  are the structure factor magnitudes derived from the measurements and calculated with

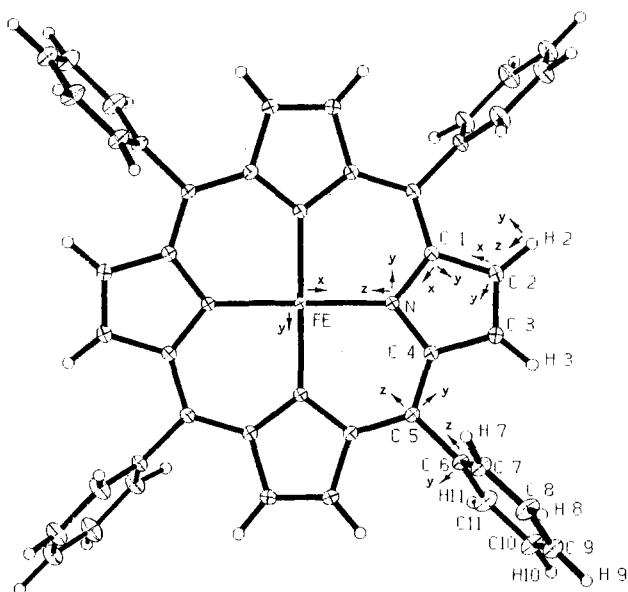


FIG. 2. Numbering of atoms and definition of local coordinate systems. For the phenyl ring atoms, the  $z$  axis is perpendicular to the plane of the ring, while the  $x$  axis bisects the C–C bonds.

TABLE II. Atomic fractional coordinates.

Atom	$x$	$y$	$z$
Fe	0.0	0.0	0.0
N	0.113 51(9)	0.065 99(7)	– 0.002 53(9)
C(1)	0.197 62(8)	0.032 85(9)	0.016 62(9)
C(2)	0.262 30(10)	0.103 46(10)	0.016 04(11)
C(3)	0.217 46(9)	0.179 77(9)	– 0.007 25(11)
C(4)	0.125 04(9)	0.156 12(9)	– 0.016 99(9)
C(5)	0.057 12(10)	0.218 49(11)	– 0.030 30(10)
C(6)	0.082 31(8)	0.311 80(9)	– 0.055 53(11)
C(7)	0.104 54(10)	0.332 58(10)	– 0.151 30(11)
C(8)	0.129 81(11)	0.419 04(10)	– 0.176 61(12)
C(9)	0.132 93(10)	0.485 30(9)	– 0.105 82(12)
C(10)	0.110 43(10)	0.465 03(10)	– 0.010 47(12)
C(11)	0.084 89(10)	0.378 65(9)	0.014 40(11)
H(2)	0.326(2)	0.092(2)	0.030(2)
H(3)	0.242(2)	0.244(2)	– 0.017(2)
H(7)	0.102 8(15)	0.287(2)	– 0.204(2)
H(8)	0.149 5(15)	0.433 2(14)	– 0.241(2)
H(9)	0.150 2(16)	0.547 7(15)	– 0.123 (2)
H(10)	0.114 3(14)	0.516(2)	0.044 0(15)
H(11)	0.069 4(15)	0.365(2)	0.083(2)

TABLE III. Anisotropic ( $\times 10^5 \text{ \AA}^2$ ) temperature factors.<sup>a</sup> The anisotropic temperature factor is defined in the form

$$\exp[-2\pi^2\{h^2a^{*2}U_{11} + k^2b^{*2}U_{22} + l^2c^{*2}U_{33} + 2(hka^{*b}U_{12} + hla^{*c}U_{13} + klb^{*c}U_{23})\}].$$

Atom	$U_{11}$	$U_{22}$	$U_{33}$	$U_{12}$	$U_{13}$	$U_{23}$
Fe	821(11)	821(11)	1149(24)	0	0	0
N	899(37)	972(40)	1595(58)	-73(34)	-25(38)	-35(40)
C(1)	942(43)	1131(48)	1834(64)	14(35)	-152(37)	89(38)
C(2)	947(48)	1436(51)	2971(80)	-135(39)	-304(44)	73(47)
C(3)	1161(47)	1196(48)	2806(72)	-291(37)	-143(49)	243(53)
C(4)	1027(44)	1004(45)	1849(62)	-88(33)	-70(36)	140(36)
C(5)	1180(57)	929(52)	1856(67)	-133(41)	-53(39)	146(39)
C(6)	1408(54)	859(47)	1651(62)	-152(36)	-108(39)	189(43)
C(7)	2453(64)	1274(50)	1629(55)	-367(41)	313(46)	-4(43)
C(8)	3334(79)	1481(57)	1891(66)	-443(50)	519(55)	245(48)
C(9)	2476(63)	1249(59)	2317(65)	-456(42)	102(48)	286(43)
C(10)	3150(68)	1305(49)	2122(72)	-581(46)	-70(58)	-124(50)
C(11)	3170(70)	1332(52)	1625(62)	-518(48)	20(49)	-38(43)

<sup>a</sup> All hydrogen temperature factors fixed at the value of  $0.035 \text{ \AA}^2$  obtained in the spherical atom refinement.

free atom scattering factors, respectively.

Since  $F_{\text{obs}}$  has a contribution from the aspherical as well as the spherical charge density, its phase is generally not equal to that calculated in the spherical approximation.<sup>32,33</sup> The phase factor  $\phi$  as calculated in the final cycle of the multipole refinement was therefore used as the phase of  $F_{\text{obs}}$ .

Structural parameters from the multipole refinement were used to obtain  $F(\text{calc})$ , while the scale factor was adjusted (by less than 1%) to give zero deformation density at the iron atom position. The standard deviation at a general position not in the vicinity of the atomic nuclei is estimated at  $0.04 e/\text{\AA}^{-3}$ .

The map through the average porphyrin plane, based on reflections with  $\sin \theta/\lambda < 0.7 \text{ \AA}^{-1}$ , (Fig. 3) shows lone pair peaks at the nitrogen atoms and density accumulation in all C-C and C-N bonds. As the molecule is ruffled the pyrrole ring atoms are displaced from the best porphyrin plane (Table VI); the electron density section through the pyrrole ring atoms is shown in Fig. 4. The left and right sides of the pyrrole densities are remarkably similar and background away from the atoms is very small, supporting the quality of the data set. As in our previous studies of porphyrins the peripheral C<sub>2</sub>-C<sub>3</sub> bond of the pyrrole ring shows a more pro-

TABLE IV. Bond distances ( $\text{\AA}$ ).

Fe-N	1.9666(15)	N-C <sub>1</sub>	1.3792(17)
N-C <sub>4</sub>	1.3752(16)	C <sub>1</sub> -C <sub>2</sub>	1.4341(20)
C <sub>1</sub> -C <sub>5</sub> <sup>Ia</sup>	1.3959(21)	C <sub>2</sub> -C <sub>3</sub>	1.3638(23)
C <sub>3</sub> -C <sub>4</sub>	1.4350(18)	C <sub>4</sub> -C <sub>5</sub>	1.3929(20)
C <sub>5</sub> -C <sub>6</sub>	1.4885(21)	C <sub>6</sub> -C <sub>7</sub>	1.3960(21)
C <sub>6</sub> -C <sub>11</sub>	1.3899(21)	C <sub>7</sub> -C <sub>8</sub>	1.3932(20)
C <sub>8</sub> -C <sub>9</sub>	1.3920(21)	C <sub>9</sub> -C <sub>10</sub>	1.3897(26)
C <sub>10</sub> -C <sub>11</sub>	1.3918(20)		
C <sub>2</sub> -H <sub>2</sub>	0.991(26)	C <sub>3</sub> -H <sub>3</sub>	1.046(24)
C <sub>7</sub> -H <sub>7</sub>	0.998(26)	C <sub>8</sub> -H <sub>8</sub>	0.954(26)
C <sub>9</sub> -H <sub>9</sub>	0.999(24)	C <sub>10</sub> -H <sub>10</sub>	1.067(23)
C <sub>11</sub> -H <sub>11</sub>	0.999(24)		

<sup>a</sup>Symmetry code I:  $-y, x, -z$ .

nounced peak than the other pyrrole bonds, indicating a larger double bond character. The difference with the other bond peaks is especially pronounced in the perpendicular sections through bond midpoint [Fig. 4(b)].

The negative, electron deficient, regions along the Fe-N bonds in Fig. 3 indicate a depopulation of the crystal-field destabilized  $d_{x^2-y^2}$  orbital relative to the spherical atom. Similarly, the peaks along the bisectors of the Fe-N bonds represent excess population in the  $d_{xy}$  orbital. The section of the deformation density perpendicular to the porphyrin plane and bisecting the N-Fe-N bonds is shown in Fig. 5. The dominant feature in this section is the pair of (symmetry related) peaks above and below the Fe atom. This is in contrast to the corresponding section in FePc which shows a deficiency in the axial direction, corresponding to a depopulation of  $d_{z^2}$  relative to the spherical atom, as predicted for the  $^3E_g$  ground state.

TABLE V. Bond angles.

N-Fe-N <sup>Ia</sup>	90.018(13)	Fe-N-C <sub>1</sub>	127.24(9)
Fe-N-C <sub>4</sub>	127.17(9)	C <sub>1</sub> -N-C <sub>4</sub>	105.44(13)
N-C <sub>1</sub> -C <sub>2</sub>	110.51(13)	N-C <sub>1</sub> -C <sub>5</sub> <sup>IIa</sup>	125.28(12)
C <sub>2</sub> -C <sub>1</sub> -C <sub>5</sub> <sup>IIa</sup>	124.14(12)	C <sub>1</sub> -C <sub>2</sub> -C <sub>3</sub>	106.65(11)
C <sub>1</sub> -C <sub>2</sub> -H <sub>2</sub>	122(2)	C <sub>3</sub> -C <sub>2</sub> -H <sub>2</sub>	131(2)
C <sub>2</sub> -C <sub>3</sub> -C <sub>4</sub>	106.86(11)	C <sub>2</sub> -C <sub>3</sub> -H <sub>3</sub>	129(1)
C <sub>4</sub> -C <sub>3</sub> -H <sub>3</sub>	124(1)	C <sub>3</sub> -C <sub>4</sub> -N	110.47(12)
C <sub>3</sub> -C <sub>4</sub> -C <sub>5</sub>	123.44(13)	N-C <sub>4</sub> -C <sub>5</sub>	125.84(13)
C <sub>4</sub> -C <sub>5</sub> -C <sub>6</sub>	118.36(13)	C <sub>4</sub> -C <sub>5</sub> -C <sub>1</sub> <sup>I</sup>	122.47(14)
C <sub>1</sub> <sup>I</sup> -C <sub>5</sub> -C <sub>6</sub>	119.10(13)	C <sub>5</sub> -C <sub>6</sub> -C <sub>7</sub>	119.37(12)
C <sub>5</sub> -C <sub>6</sub> -C <sub>11</sub>	121.43(13)	C <sub>7</sub> -C <sub>6</sub> -C <sub>11</sub>	119.20(13)
C <sub>6</sub> -C <sub>7</sub> -C <sub>8</sub>	120.57(13)	C <sub>6</sub> -C <sub>7</sub> -H <sub>7</sub>	122(1)
C <sub>8</sub> -C <sub>7</sub> -H <sub>7</sub>	118(1)	C <sub>7</sub> -C <sub>8</sub> -C <sub>9</sub>	119.75(13)
C <sub>7</sub> -C <sub>8</sub> -H <sub>8</sub>	121(1)	C <sub>9</sub> -C <sub>8</sub> -H <sub>8</sub>	119(1)
C <sub>8</sub> -C <sub>9</sub> -C <sub>10</sub>	119.90(13)	C <sub>8</sub> -C <sub>9</sub> -H <sub>9</sub>	120(1)
C <sub>10</sub> -C <sub>9</sub> -H <sub>9</sub>	120(1)	C <sub>9</sub> -C <sub>10</sub> -C <sub>11</sub>	120.15(13)
C <sub>9</sub> -C <sub>10</sub> -H <sub>10</sub>	120(1)	C <sub>11</sub> -C <sub>10</sub> -H <sub>10</sub>	120(1)
C <sub>10</sub> -C <sub>11</sub> -C <sub>6</sub>	120.43(14)	C <sub>10</sub> -C <sub>11</sub> -H <sub>11</sub>	119(1)
C <sub>6</sub> -C <sub>11</sub> -H <sub>11</sub>	120(1)		

<sup>a</sup>Symmetry code I:  $-y, x, -z$ ; II:  $y, -x, -z$ .

TABLE VI. Least-squares plane and distances from plane (Å) (\* atoms not included in definition of planes).

1. Averaged porphyrin plane through Fe			
$0.0x + 0.0y + 1.0z = 0.0$			
Fe	0.0		
N	-0.035	C <sub>1</sub>	+0.229
C <sub>2</sub>	0.221	C <sub>3</sub>	-0.100
C <sub>4</sub>	-0.234	C <sub>5</sub>	-0.417
2. Pyrrole plane			
$-0.1489x + 0.1651y + 0.9750z + 0.1265 = 0.0$			
N	0.003	C <sub>1</sub>	-0.010
C <sub>2</sub>	0.013	C <sub>3</sub>	-0.011
C <sub>4</sub>	0.005	C <sub>5</sub> *	0.132
3. Phenyl plane			
$0.9547x - 0.2283y + 0.1909z + 0.0391 = 0.0$			
C <sub>6</sub>	0.004	C <sub>7</sub>	-0.001
C <sub>8</sub>	-0.002	C <sub>9</sub>	0.002
C <sub>10</sub>	0.001	C <sub>11</sub>	-0.004
C <sub>5</sub> *	0.029	H <sub>7</sub> *	-0.009
H <sub>8</sub> *	0.062	H <sub>9</sub> *	-0.009
H <sub>10</sub> *	0.025	H <sub>11</sub> *	0.002

A theoretical study of the electron distribution in iron-(II)porphyrin was reported recently by Rohmer,<sup>16</sup> who calculated both the  ${}^3A_{2g}$  and the  ${}^3E_gA$  states. Additional calculations allowing for mixing of excited configurations with these SCF ground states had little effect on the electron density maps. The theoretical, static, electron density distributions of the two configurations differ little in the plane of the

porphyrin ring [Figs. 6(a) and 6(b)], in accordance with the equal occupancy of the  $d_{xy}$  orbital in the two configurations. In the perpendicular section [Figs. 6(c) and 6(d)], however, the  ${}^3A_{2g}$  distribution has excess density along  $z$ , while  ${}^3E_gA$  shows a deficiency, as observed in FePc. The large peak along the  $z$  direction in the observed distribution suggests a relatively low contribution of the  ${}^3E_gA$  state to the ground state configuration of the complex.

### Atomic multipole populations

Multipole populations from the aspherical atom refinement are listed in Table VII. Residual electron density maps calculated after the multipole refinement (Fig. 7) show some density around the iron atom in the molecular plane at about  $25^\circ$  from the Fe–N bonds. This residual density is a result of the  $4/m\bar{m}$  symmetry assumed for the Fe atom in the multipole refinement. However, a refinement in which this constraint was lifted showed the deviation from  $4/m\bar{m}$  symmetry to be not significant. There are also negative areas at about  $2\text{ \AA}$  from the Fe atom along the  $z$  axis [Fig. 7(b)] which have not been modeled by the basis functions as they are too far removed from the atomic centers. Except for these feature the residual maps are essentially flat.

The positive value of the population coefficient,  $P_{20}$ , on the iron atom accounts for much of the density accumulation along the  $z$  axis, while the negative value of  $P_{4+}$  represents the redistribution of the electrons away from the axial to the bisecting directions in the porphyrin plane.

In order to examine the possibility that the  $z$ -axis peak results from a small displacement of the Fe atom from the center of the molecule, two refinements were done in which the iron was displaced by  $\Delta z = \pm 0.003$  (0.041 Å) and  $\pm 0.005$  (0.069 Å) from the origin. These two refinement did not improve the agreement factors and did not reduce the value of the population parameter  $P_{20}$ . We conclude that the observed maximum along  $z$  is the not a result of disorder in the crystals of FeTPP.

The iron valence electron population of 7.18(11) corresponds to a donation of 1.18 electrons to the  $Fe^{2+}$  ion. The phenyl group and the pyrrole rings have net charges of  $-0.22$  and  $-0.27$ , respectively, while the Fe atom and the meso carbon are positively charged. The charge on the Fe atom of 0.82(12) is almost exactly balanced by the negative charge on the four nitrogen atoms.

### $d$ -electron population from the multipole parameters

The populations of the  $d$  orbitals can be derived directly from the multipole parameters as described elsewhere.<sup>30</sup> Results are listed in Table VIII together with those of FePc,<sup>18</sup> theoretical values,<sup>10,11,16</sup> the populations for the spherical Fe(II) atom, and several ionic configurations. Since the deformation functions used for the iron atom in FePc were Slater-type rather than Hartree–Fock functions the absolute values of the populations in the two compounds may not be directly comparable. Instead the relative values, which are much less sensitive to the choice of radial function, may be compared. While the FePc populations generally agree with

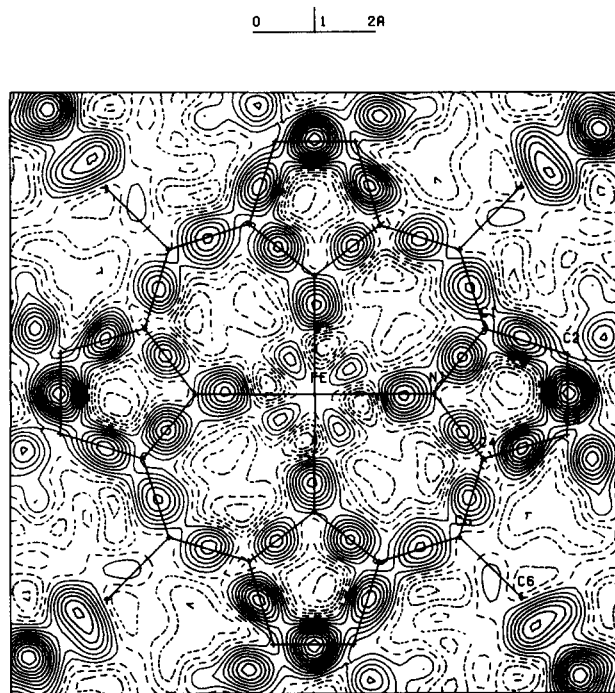


FIG. 3. Deformation density section through the porphyrin plane, calculated with phases from the multipole refinement. Reflections with  $\sin \theta / \lambda < 0.7\text{ \AA}^{-1}$  included. Contours at  $0.05 e\text{ \AA}^{-3}$ . Zero and negative contours broken.

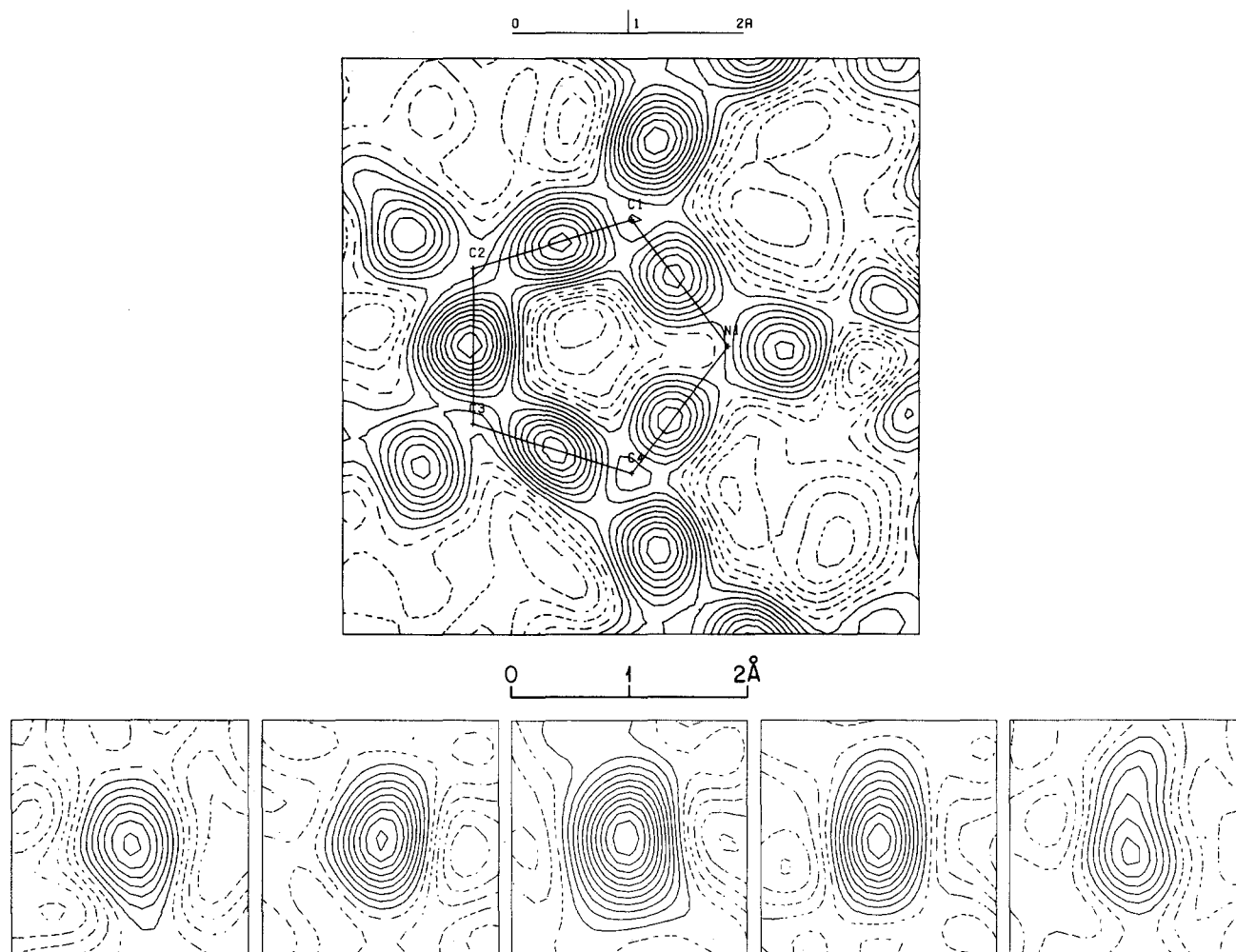


FIG. 4. (a) Deformation density in the plane of the pyrrole ring. Details as in Fig. 3. (b) Sections perpendicular bond through bond midpoint for N-C<sub>1</sub>, C<sub>1</sub>-C<sub>2</sub>, C<sub>2</sub>-C<sub>3</sub>, C<sub>3</sub>-C<sub>4</sub>, and C<sub>4</sub>-N.

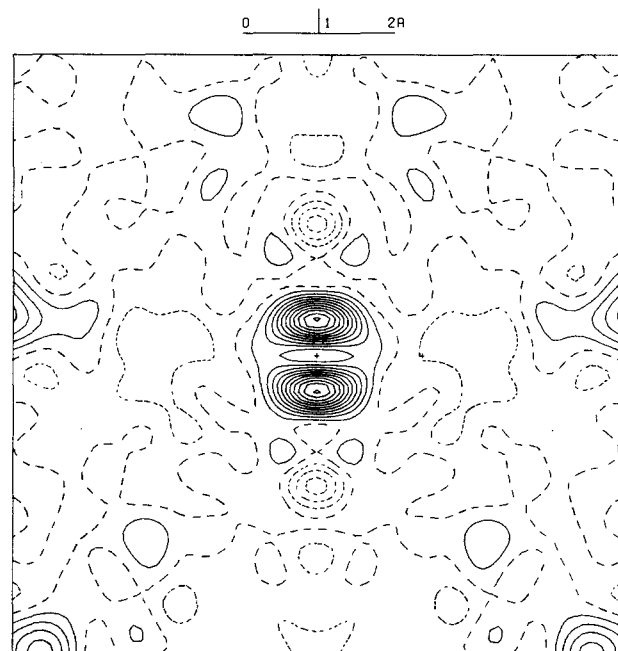


FIG. 5. Deformation density section through plane bisecting N-Fe-N bonds, perpendicular to the average porphyrin plane. Contours at  $0.10 e \text{ \AA}^{-3}$ . Other details as in Fig. 3. The Fe atom is indicated by a + sign. The porphyrin plane is horizontal.

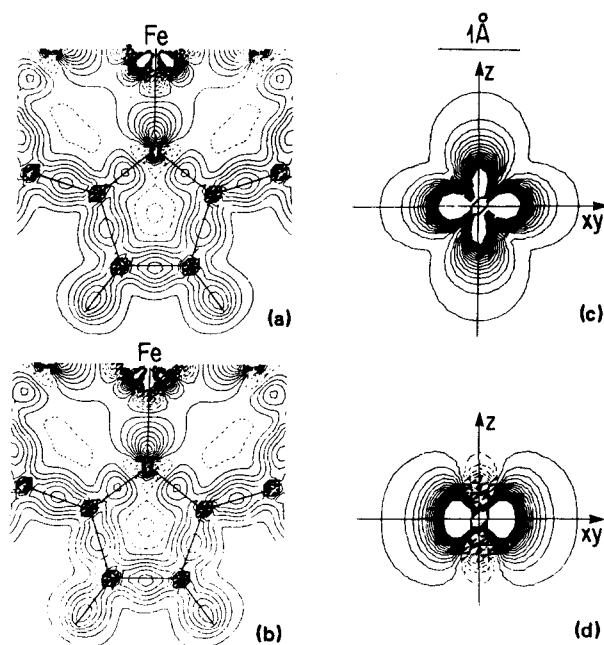


FIG. 6. Computed static deformation density maps of FeP from Ref. 16. Contours at  $0.10 e \text{ \AA}^{-3}$ . (a)  ${}^3A_{2g}$  in-plane, (b)  ${}^3E_g$  in-plane, (c)  ${}^3A_{2g}$  bisecting plane, (d)  ${}^3E_g$  bisecting plane.

TABLE VII. Multipole populations.

<b>Fe (<math>4/m\ mm</math>)</b>			
$\kappa'$	0.969(17)	$P_{20}$	0.43(6)
$P_{00}$	7.18(11)	$P_{40}$	-0.12(6)
		$P_{44+}$	-0.34(7)
<b>N (<math>mm</math>)</b>			
$n_i^a$	2,2,3	$P_{20}$	0.10(3)
$\kappa$	1.0(2)	$P_{22+}$	-0.02(4)
$\kappa'\zeta$ , bohr $^{-1}$	3.8 (not refined)		
$P_{val}$	5.21(17)	$P_{30}$	0.11(3)
$P_{10}$	0.13(4)	$P_{32+}$	-0.07(3)
<b>C<sub>1</sub>, C<sub>4</sub> (<math>m</math>)</b>			
$n_i^a$	2,2,3	$P_{20}$	-0.23(5)
$\kappa$	1.02(2)	$P_{22+}$	-0.04(4)
$\kappa'\zeta$ , bohr $^{-1}$	2.63(16)	$P_{22-}$	0.06(6)
$P_{val}$	4.09(19)	$P_{31+}$	0.00(3)
$P_{11+}$	0.02(5)	$P_{31-}$	-0.02(3)
$P_{11-}$	0.02(5)	$P_{33+}$	0.42(7)
		$P_{33-}$	0.06(5)
<b>C<sub>2</sub>, C<sub>4</sub> (<math>m</math>)</b>			
$n_i^a$	2,2,3	$P_{22+}$	-0.04(3)
$\kappa$	1.0(1)	$P_{22-}$	0.08(3)
$\kappa'\zeta$ , bohr $^{-1}$	3.2 (not refined)	$P_{31+}$	-0.02(3)
$P_{val}$	4.21(9)	$P_{31-}$	-0.02(2)
$P_{11+}$	-0.04(4)	$P_{33+}$	-0.25(3)
$P_{11-}$	0.05(3)	$P_{33-}$	-0.08(3)
$P_{20}$	-0.14(3)		
<b>C<sub>5</sub> (<math>m</math>)</b>			
$n_i^a$	2,2,3	$P_{21-}$	0.02(3)
$\kappa$	1.04(3)	$P_{22+}$	-0.14(5)
$\kappa'\zeta$ , bohr $^{-1}$	3.2 (not refined)	$P_{30}$	0.19(6)
$P_{val}$	3.71(28)	$P_{31-}$	0.02(3)
$P_{11-}$	-0.04(3)	$P_{32+}$	0.12(5)
$P_{10}$	0.03(6)	$P_{33-}$	0.0(3)
$P_{20}$	0.04(5)		
<b>C<sub>6</sub> (<math>m</math>)</b>			
$n_i^a$	2,2,3	$P_{22+}$	-0.03(5)
$\kappa$	1.0(2)	$P_{22-}$	0.01(4)
$\kappa'\zeta$ , bohr $^{-1}$	2.65(18)	$P_{31+}$	0.03(5)
$P_{val}$	4.52(14)	$P_{31-}$	-0.04(4)
$P_{11+}$	0.02(5)	$P_{33+}$	-0.40(6)
$P_{11-}$	0.05(4)	$P_{33-}$	0.01(4)
$P_{20}$	-0.37(5)		
<b>C<sub>7</sub>, C<sub>8</sub>, C<sub>9</sub>, C<sub>10</sub>, C<sub>11</sub> (<math>m</math>)</b>			
$n_i^a$	2,2,3	$P_{22+}$	-0.04(2)
$\kappa$	1.016(9)	$P_{22-}$	-0.02(2)
$\kappa'\zeta$ , bohr $^{-1}$	3.2 (not refined)	$P_{31+}$	-0.04(2)
$P_{val}$	4.22(5)	$P_{31-}$	-0.01(2)
$P_{11+}$	0.02(2)	$P_{33+}$	-0.25(2)
$P_{11-}$	-0.01(2)	$P_{33-}$	0.01(2)
$P_{20}$	-0.22(2)		
<b>Hydrogens</b>			
$n_i^a$	1	$P_{val}$	0.72(3)
$\kappa$	1.4 (not refined)	$P_{10}$	0.18(4)
$\kappa'\zeta$ , bohr $^{-1}$	1.0 (not refined)		

<sup>a</sup> Exponent of  $r$  in radial function.  $R(r) = Nr^{n(l)} \exp(-\kappa'\zeta r)$  for dipole, quadrupole, and octapole terms, respectively.

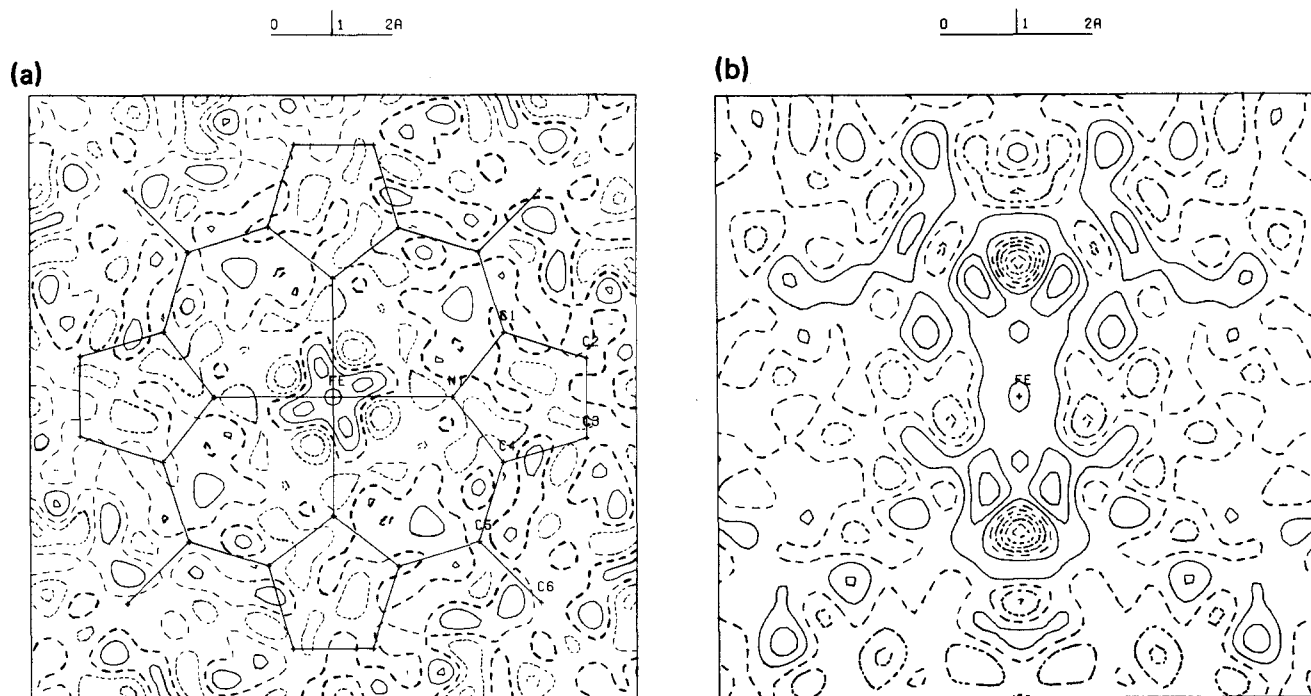


FIG. 7. Residual maps after multipole refinement,  $\sin \theta / \lambda < 0.7 \text{ \AA}^{-1}$ . Contours at  $0.05 e \text{ \AA}^{-3}$ . (a) Porphyrin plane, (b) bisecting plane as defined in Fig. 5.

the theoretical results for the  ${}^3E_g A$  state, no such agreement is found for the present results on FeTPP.

The observed relative populations are intermediate between those of the two ionic  ${}^3E_g$  configurations. We may use the values for the  $d_{xy}$  and  $d_{x^2-y^2}$  orbitals to estimate the relative contribution of the two configurations to the electronic ground state. If these two states are the principal contributors, relative contributions of 40.5% and 59.5% for  ${}^3E_g A$  and  ${}^3E_g B$ , respectively, are obtained. This is in qualita-

tive agreement with the model of Obara and Kashiwagi,<sup>12</sup> but with a much larger contribution from the latter configuration than predicted theoretically.

The population of the  $d_{x^2-y^2}$  orbital which is destabilized according to crystal field theory is similar to that observed in our previous studies.<sup>19-21</sup> It is mainly a result of  $\sigma$  donation from the ligand orbitals, though polarized neutron data on CoPc indicate that mixing of excited states may also be a contributing factor.<sup>34</sup>

TABLE VIII. (A) Experimental and theoretical  $d$ -orbital occupancies with those of spherical Fe atom. (B)  $d$ -orbital occupancies for triplet state ionic configurations.

(A)	FeTPP	FePc <sup>a</sup>	Theory EH <sup>b</sup> ${}^3E_g A$	Theory SCF-CI <sup>c</sup> ${}^3A_{2g}$	${}^3E_g A$	Spherical
$d_{x^2-y^2}$	0.43(13)(6.0%)	0.70(7)(12.9%)	0.896(12.8%)	0.18(2.9%)	0.18(2.9%)	1.2(20%)
$d_{x^2}$	1.70(11)(23.7%)	0.93(6)(17.1%)	1.071(15.3%)	1.94(31.7%)	0.99(16.1%)	1.2(20%)
$d_{xz}, d_{yz}$	3.54(14)(49.3%)	2.12(7)(39.1%)	3.054(43.5%)	1.98(32.3%)	2.96(48.1%)	2.4(40%)
$d_{xy}$	1.50(13)(20.9%)	1.68(10)(30.9%)	1.994(28.4%)	2.02(33.0%)	2.02(32.8%)	1.2(20%)
(B)	${}^3A_{2g}$	${}^3E_g A$	${}^3E_g B$	${}^3B_{2g}$		
$d_{x^2-y^2}$	0	0	0	0		
$d_{x^2}$	2 (33%)	1 (17%)	2 (33%)	1 (17%)		
$d_{xz}, d_{yz}$	2 (33%)	3 (50%)	3 (50%)	4 (67%)		
$d_{xy}$	2(33%)	2 (33%)	1 (17%)	1 (17%)		

<sup>a</sup> Reference 18.

<sup>b</sup> Extended Hückel; Zerner, Gouterman, and Kobayashi (Ref. 11).

<sup>c</sup> Rohmer (Ref. 16).

### Electric field gradient at the Fe nucleus

The electric field gradient (EFG) at the iron nucleus can be calculated from the least-squares population of the multipoles.<sup>35</sup> The elements of the field gradient tensor are defined by

$$V_{ij} = \int \rho(\mathbf{r}) \hat{V}_{ij} d\mathbf{r},$$

where the operator  $\hat{V}_{ij}$  is given by

$$\hat{V}_{ij} = -(3r_i r_j - r^2 \delta_{ij})/r^5.$$

The electric field gradient is also accessible through the quadrupole splitting of the Mössbauer resonance lines which is a function of  $V_{zz}$  and the asymmetry parameter  $\eta$  defined as  $V_{xx} - V_{yy}$ . Since the iron atom in FeTPP is located on a fourfold inversion axis the asymmetry parameter  $\eta$  is zero. The angular integration for  $V_{zz}$  gives a term dependent on the multipole population parameter  $P_{20}$  only, while the radial integration requires evaluation of the radial integral  $\int_0^\infty R(r)/r dr$ ,<sup>35</sup> where  $R(r)$  is the radial part of the  $d$ -orbital density basis functions. Evaluation of this integral for the HF type radial functions used in this work leads to a value of  $5.2 \text{ bohr}^{-3}$ .

Taking into account that  $\kappa = 0.97$ , the corresponding value of  $V_{zz}$  is  $-13.4 \times 10^{15} \text{ esu/cm}^3$ , which may be compared directly with the Mössbauer results. Using appropriate conversion factors and Sternheimer antishielding factors  $\gamma_\infty$  and  $R$  of  $-10$  and  $0.22$ , respectively,<sup>36</sup> gives a Mössbauer hyperfine splitting of  $-6.5(9) \text{ mm/s}$ , compared with experimental results of  $1.32$  and  $1.52 \text{ mm/s}$ .<sup>4,5</sup>

Thus, unlike previous studies on iron pyrite, FeTPP (OMe) and FePc which produced agreement between the x-ray and the spectroscopic results, within the considerable experimental errors of the x-ray value, a discrepancy is found in the present work. However, we note that the comparison is affected by uncertainties in the shielding parameters as pointed out by Lang *et al.*<sup>5</sup>

The large negative x-ray value is a direct result of the  $P_{20}$  multipole population parameter, which is related to the  $d$ -orbital occupancies by the expression  $3.64 P_{20} = P_{z^2} + P_{xz} - P_{x^2-y^2} - P_{xy}$ . Thus, the Mössbauer results suggest less electron density along the  $z$  direction and more density in the  $xy$  plane than observed in the present experiment.

### DISCUSSION

Even though FeTPP crystallizes in a noncentrosymmetric space group, the lack of noise in the regions away from the atoms (Figs. 3–5) and the observed noncrystallographic symmetry in the deformation section through the plane of the pyrrole ring (Fig. 4) support the quality of the results, and indicate that the estimate of the standard deviation at a general position ( $0.04 e \text{ \AA}^{-3}$ ) is reasonable. Nevertheless, systematic errors in the observed amplitudes, which are not accounted for in the estimate of the standard deviation, may produce artifacts, in particular, near heavier atoms<sup>37</sup> or positions of high multiplicity. Thus, the large peak on the  $z$  axis (Fig. 5) has a larger uncertainty than other features in the density maps.

When the experimental populations are compared with

the theoretical values of  ${}^3A_{2g}$  and  ${}^3E_gA$  [Table VIII(A)], the main difference with either configuration occurs for the  $d_{xy}$  populations which are much lower in the experiment, while  $d_{xz,yz}$  agrees with  ${}^3E_gA$  and  $d_{z^2}$  is intermediate between  ${}^3A_{2g}$  and  ${}^3E_gA$ . The alternative explanation discussed above is a 60–40 admixture of  ${}^3E_gB$  and  ${}^3E_gA$ . However, theoretical calculations typically show the former configuration to be considerably higher in energy.

A lowering of the  $z$ -axis peak would bring the results in closer agreement with the Mössbauer data. However, in order to get agreement with either the  ${}^3A_{2g}$  or the  ${}^3E_gA$  populations, we would also have to assume that the  $d_{xy}$  population has been underestimated in the experimental results, as both configurations have a 33% population in this orbital vs 20.9% for the experimental result.

Perhaps the most evident conclusion to be drawn from the experimental results is that they represent a mixing of several ground state configurations, with a smaller than 50% contribution from  ${}^3E_gA$ . This implies different electronic ground states for FeTPP and FePc in the crystalline matrix. This result is not unreasonable since there is abundant evidence that the energy levels are closely spaced and will be affected by differences in crystal packing.<sup>1,7</sup>

A recent study<sup>38</sup> indicates that Fe(II) octaethyl porphyrin (FeOEP) crystallizes in the more favorable centrosymmetric space group  $P\bar{1}$  with half a molecule in the asymmetric unit. We intend to perform a charge density analysis of FeOEP as a continuation of the studies described here.

### ACKNOWLEDGMENTS

The work reported here was supported by the National Institutes of Health (HL2388404) and the National Science Foundation (CHE8403428). We would like to thank Dr. Takenaka and Professor Sasada of the Tokyo Institute of Technology for the drawing program DCMS82 used in the preparation of Figs. 1 and 2. We are indebted to Dr. M. M. Rohmer for providing the theoretical  $d$ -orbital populations given in Table VIII.

<sup>1</sup>P. D. W. Boyd, D. A. Buckingham, R. F. McMeeking, and S. Mitra, *Inorg. Chem.* **18**, 3585 (1979).

<sup>2</sup>C. G. Barraclough, R. L. Martin, S. Mitra, and R. C. Sherwood, *J. Chem. Phys.* **53**, 1643 (1970).

<sup>3</sup>J. P. Collman, J. L. Hoard, N. Kim, G. Lang, and C. A. Reed, *J. Am. Chem. Soc.* **97**, 2676 (1975).

<sup>4</sup>H. Kobayashi, Y. Maeda, and Y. Yanagawa, *Bull. Chem. Soc. Jpn.* **43**, 2342 (1970).

<sup>5</sup>G. Lang, K. Spartalian, C. A. Reed, and J. P. Collman, *J. Chem. Phys.* **69**, 5424 (1978).

<sup>6</sup>H. Goff, G. N. La Mar, and C. A. Reed, *J. Am. Chem. Soc.* **99**, 3641 (1977).

<sup>7</sup>J. Mispelter, M. Momenteau, and J. M. Lhoste, *J. Chem. Phys.* **72**, 1003 (1980).

<sup>8</sup>T. Kitagawa and J. Teraoka, *Chem. Phys. Lett.* **63**, 443 (1979).

<sup>9</sup>M. J. Stillman and A. J. Thomson, *J. Chem. Soc. Faraday Trans.* **1974**, 790.

<sup>10</sup>M. Zerner and M. Gouterman, *Theor. Chim. Acta (Berlin)* **4**, 44 (1966).

<sup>11</sup>M. Zerner, M. Gouterman, and H. Kobayashi, *Theor. Chim. Acta*, **6**, 363 (1966).

<sup>12</sup>S. Obara and H. Kashiwagi, *J. Chem. Phys.* **77**, 3155 (1982).

<sup>13</sup>A. Dedieu, M. M. Rohmer, and A. Veillard, *Adv. Quantum Chem.* **16**, 43 (1982).

<sup>14</sup>D. E. Ellis and Z. Berkovitch-Yellin, *J. Appl. Phys.* **52**, 1633 (1981).

- <sup>15</sup>S. F. Sontum, D. A. Case, and M. Karplus, *J. Chem. Phys.* **79**, 2881 (1983).
- <sup>16</sup>M. M. Rohmer, *Chem. Phys. Lett.* **116**, 44 (1985).
- <sup>17</sup>H. Kobayashi and Y. Yanagawa, *Bull. Chem. Soc. Jpn.* **45**, 450 (1972).
- <sup>18</sup>P. Coppens and L. Liang, *J. Chem. Phys.* **81**, 1983 (1984).
- <sup>19</sup>E. D. Stevens, *J. Am. Chem. Soc.* **103**, 5087 (1981).
- <sup>20</sup>C. Lecomte, D. L. Chadwick, P. Coppens, and E. D. Stevens, *Inorg. Chem.* **22**, 2982 (1983).
- <sup>21</sup>C. Lecomte, R. Blessing, and P. Coppens (to be published).
- <sup>22</sup>R. Blessing, P. Coppens, and P. J. Becker, *J. Appl. Crystallogr.* **7**, 488 (1974).
- <sup>23</sup>L. E. McCandlish, G. H. Stout, and L. C. Andrews, *Acta Crystallogr. Sect. A* **31**, 245 (1975).
- <sup>24</sup>P. Coppens, L. Leiserowitz, and D. Rabinovitch, *Acta Crystallogr.* **18**, 1035 (1965).
- <sup>25</sup>N. K. Hansen (private communication).
- <sup>26</sup>*International Tables for X-ray Crystallography* (Kynoch, Birmingham, England, 1974), Vol. 4.
- <sup>27</sup>R. F. Stewart, E. R. Davidson, and W. T. Simpson, *J. Chem. Phys.* **42**, 3175 (1965).
- <sup>28</sup>N. K. Hansen and P. Coppens, *Acta Crystallogr. Sect. A* **34**, 909 (1974).
- <sup>29</sup>E. Clementi and D. L. Raimondi, *J. Chem. Phys.* **38**, 2686 (1963).
- <sup>30</sup>A. Holladay, P. Leung, and P. Coppens, *Acta Crystallogr. Sect. A* **39**, 377 (1983).
- <sup>31</sup>W. R. Scheidt and C. A. Reed, *Chem. Rev.* **81**, 543 (1981).
- <sup>32</sup>P. Coppens, *Acta Crystallogr. Sect. B* **30**, 255 (1974).
- <sup>33</sup>J. M. Savariault and M. S. Lehmann, *J. Am. Chem. Soc.* **102**, 1298 (1980).
- <sup>34</sup>P. Coppens, A. Holladay, and E. D. Stevens, *J. Am. Chem. Soc.* **104**, 3546 (1982).
- <sup>35</sup>E. D. Stevens, M. L. DeLucia, and P. Coppens, *Inorg. Chem.* **19**, 813 (1980).
- <sup>36</sup>S. L. Finklea, L. Cathey, and E. L. Amma, *Acta Crystallogr. Sect. A* **32**, 529 (1976).
- <sup>37</sup>J. M. Troup, M. W. Extine, and R. F. Ziolo, in *Electron Distributions and the Chemical Bond*, edited by P. Coppens and M. B. Hall (Plenum, New York, 1982), p. 294.
- <sup>38</sup>S. H. Strauss, M. E. Silver, K. M. Long, R. G. Thompson, R. A. Hudgens, K. Spartalian, and J. A. Ibers, *J. Am. Chem. Soc.* **107**, 4207 (1985).
- <sup>39</sup>See AIP document no. PAPS JCPSA-84-6969-17 for 17 pages of structure factors. Order by PAPS number and journal reference from American Institute of Physics, Physics Auxiliary Publication Service, 335 East 45th Street, New York, NY 10017. The price is \$1.50 for each microfiche (98 pages) or \$5.00 for photocopies of up to 30 pages, and \$0.15 for each additional page over 30 pages. Airmail additional. Make checks payable to the American Institute of Physics.